AIR MOVEMENT & VENTILATION CONTROL WITHIN BUILDINGS

12th AIVC Conference, Ottawa, Canada
24-27 September, 1991

POSTER 47

Definition of the Flow Parameters at the Room Inlet Device
- Measurements and Calculations -

M. Ewert, U. Renz, N. Vogl, M. Zeller
Lehrstuhl für Wärmeübertragung und Klimatechnik
RWTH Aachen
D - 5100 Aachen

Synopsis
Due to the limitations of computer storage and time the flow boundary conditions at an air inlet device have to be specified for numerical simulations of air flow patterns in rooms. With regard to this the present work gives velocity measurements near an industrial air inlet using a Laser-Doppler-Anemometer.
From the stochastic velocity data the time-averaged velocity components, standard deviation and turbulent kinetic energy are evaluated. Furthermore the dissipation rate of the turbulent kinetic energy is determined from the time scale of the autocorrelation coefficient and alternativly from the frequency spectrum of turbulence. The assumptions required for the calculations are discussed.
Finally, measured data at a distance of one meter from the air inlet are compared with the numerically predicted velocity field and turbulence parameters, which are based on boundary conditions of a simplified inlet. Comparisons of numerically predicted air flow in the occupied zone show a significant difference depending on whether measured boundary conditions or those for a simplified slit are used. In particular the predicted turbulent kinetic energy for the simplified slit boundary condition is twice that for the measured boundary condition.

1. Measurement Technique and Testcase

With a one-component Argon-Ion-Laser-System the three local velocity components are measured. The laser and data processing system, the optical sensor, connected with the laser and a Burst Spectrum Analyser (BSA) by a fiber system, and a traversing device are described in /1/.
The measurements are carried out in a testroom with an air inlet device specified in the IEA-Annex 20 work /2/, /3/. The dimensions of the testroom and location of the imaginary entrance box, where Laser-Doppler-Anemometer (LDA) measurements are carried out, and the simplified slit inlet are shown in figure 1.

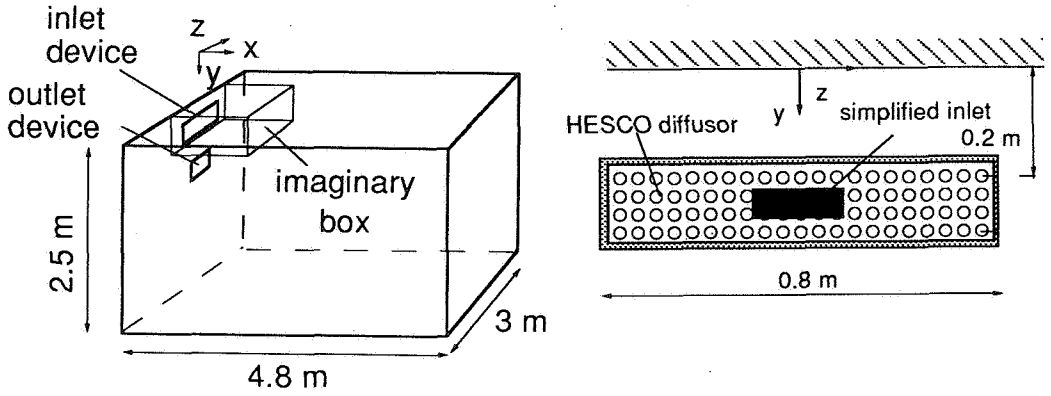

Figure 1: Dimensions of the testroom, industrial inlet device, simplified slit inlet and imaginary box

2. Determination of Turbulence Parameters

All statistical values of interest are calculated from the stochastic velocity data measured in the three directions of the testroom. The turbulent kinetic energy k is obtained from the velocity fluctuations as follows:

$$k = \frac{1}{2} \sum_{i=1}^{3} \overline{u_i'^2} \qquad (1)$$

Because the local gradients of the velocity fluctuations can not be measured simultaneously with available equipment the dissipation of turbulent kinetic energy ε can only be determined indirectly. However, different models to describe the dissipation rate as a function of known variables exist. Two suitable but rather simplifying models are found and adopted to the use of LDA measurements.
The first one is given by Rotta /4/.

$$\varepsilon = 0.165 \frac{k^{3/2}}{L} \tag{2}$$

This model relates ε with turbulent kinetic energy and length scale L. The constant depends on the definition of the length scale, which can be calculated from the spatial correlation functions and using Taylor's hypothesis from the autocorrelation function. Rotta has defined the length scale as

$$L = \frac{3}{8k} \int_0^{\infty} (R_{11}(r_2)\, \overline{u_1'^2} + R_{22}(r_2)\, \overline{u_2'^2} + R_{33}(r_2)\, \overline{u_3'^2}\,)\, dr_2 \tag{3}$$

where 1 is the main flow direction and 2 the direction of the greatest gradient. $R_{11}(r_2)$ and $R_{33}(r_2)$ are lateral and $R_{22}(r_2)$ longitudinal correlations. Assuming isotropic turbulence a relation between longitudinal and lateral correlations can be established, and with Taylor's hypothesis the spatial correlation $R_{ii}(\mathbf{r})$ and autocorrelation $R_{ii}(\tau\bar{U})$ are identical. Herein $\mathbf{r}$ is the spatial distance vector, $\bar{U}$ the mean velocity vector and τ the correlation time. The longitudinal and lateral correlation coefficients of equation (3) are found from the measured autocorrelation coefficient

$$R_{ii}(\tau) = \frac{\overline{u_i'(t)\, u_i'(t+\tau)}}{\left(\overline{u_i'(t)^2} \cdot \overline{u_i'(t+\tau)^2}\right)^{1/2}} \tag{4}$$

Figure 2 shows the measured autocorrelation function $R_{11}(\tau)$ smoothed by splines.

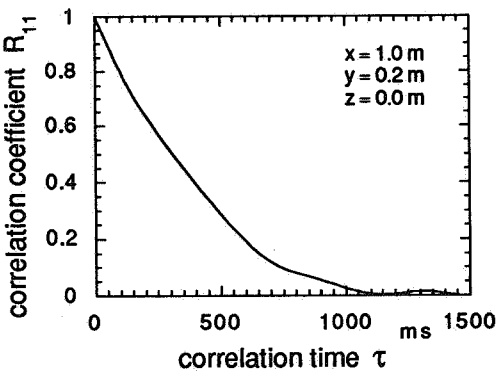

Figure 2: Measured autocorrelation function $R_{11}(\tau)$

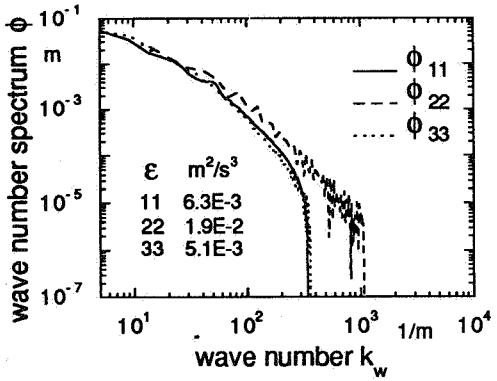

Figure 3: Wave number spectra in three directions and mean dissipation rate

The length scale, equation (3), is derived by integration of the calculated lateral autocorrelation coefficients R_{11} and R_{33} from the velocity components 1 and 3, and of the longitudinal coefficient R_{22} from the velocity component 2. More details are given in /1/, /5/.

The second model given by Hinze /6/ is based on the wave number spectrum of turbulence. If we assume isotropic turbulence the dissipation rate is given by

$$\varepsilon = 15\,\nu \int_0^\infty k_w^2 \phi_{ii}(k_w)\, dk_w, \tag{5}$$

where $\phi_{ii}(k_w)$ is the one dimensional wave number spectrum and ν the kinematic viscosity. With the following relation between the wave number k_w and the frequency ω and a simplification of the wave velocity U_c

$$k_w = \frac{\omega}{U_c} \qquad U_c = \bar{U} + \frac{\overline{ku'}}{k} \approx \bar{U} \tag{6}$$

the dissipation rate becomes

$$\varepsilon = \frac{15\nu}{\overline{U}^2} \int_0^\infty \omega^2 \phi_{ii}(\omega)\, d\omega. \tag{7}$$

The frequency spectrum $\phi_{ii}(\omega)$ is calculated from the longitudinal autocorrelation function

$$\phi_{ii}(\omega) = \frac{2\,\overline{u_i'^2}}{\pi} \int_0^\infty R_{ii}(\tau) \exp(-i\omega\tau)\, d\tau \tag{8}$$

By substituting $R_{ii}(\tau)$ with the longitudinal correlation calculated with the assumption of isotropic turbulence, we obtain three different frequency spectra and three different dissipation rates from measurements in the three directions as shown in figure 3. This indicates the nonisotropic structure of the flow. In order to get a mean value for ε which can be used as a boundary condition for the numerical simulations we introduce the following averaging

$$\varepsilon = \frac{1}{2k} \sum_{i=1}^{3} \varepsilon_{ii}\, \overline{u_i'^2} \tag{9}$$

The reason for weighting with velocity fluctuations is that the dissipation rate increases with increasing fluctuation velocities.

3. Results

3.1 Measurements and Calculations Near Air Inlet

The numerical simulations were carried out with the FLUENT code /7/ by solving the conservation equations for mass, momentum, turbulent kinetic energy and dissipation of the turbulent kinetic energy.

For the numerical simulations the real geometrical inlet conditions of experiments are simplified by a slit inlet. The mean velocity and the momentum of the slit sketched in figure 1 are the same as for the real inlet device. Comparisons of numerical predictions using different finite difference schemes and measured values of velocity, turbulent kinetic energy and dissipation rate at the symmetry plane of

the imaginary box are shown in figure 4 for an air exchange rate of 6 h^{-1} (flow rate 0,063 m^3/s).
Measurements yield higher velocities than simulations with the Power-Law (PL) and the QUICK scheme.The PL scheme results in a lower maximum velocity due to its higher numerical diffusion. A strong difference is also seen for turbulent kinetic energy. The measured values are ten times higher than calculations with PL, and two times higher than those with the QUICK scheme.
Comparison of the dissipation rate is quite difficult, because "measured" data are evaluated with simplifying models. The resulting values for the two models described above differ by more than one order of magnitude, but both curves indicate the same tendency. Results from numerical simulations are completely different. The profiles from the QUICK scheme are again closer to measurements.
Additional k- and ε-profiles calculated from the velocity magnitude as given in equation (10) are included in figure 4 for a turbulence intesity of Tu = 0.1.

$$k = 1.5\,(\bar{U}\,Tu)^2\,;\quad \varepsilon = c_\mu^{3/4} k^{1.5}/L \qquad c_\mu = 0.09; \qquad L = y \tag{10}$$

These formulas are normally used as boundary conditions if only the velocity values are available.

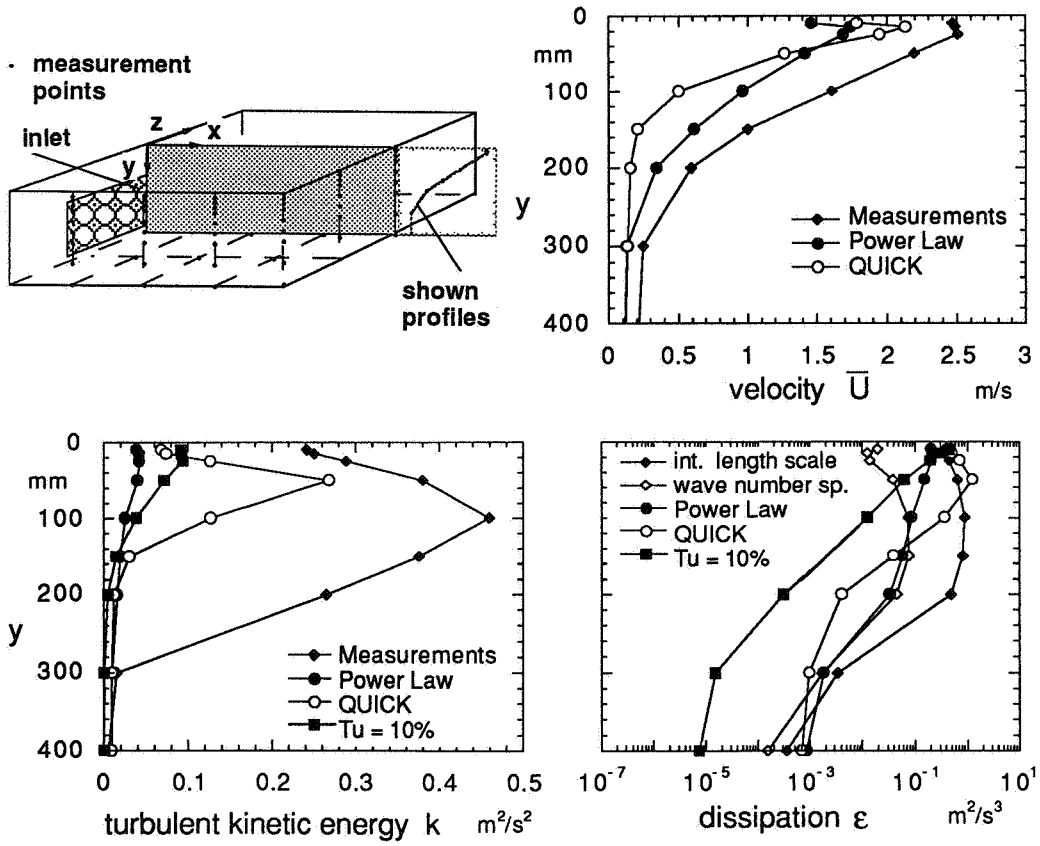

Figure 4: Comparison between measurements and numerical calculations at the symmetry plane of the imaginary box

3.2 Numerical Simulations of Room Air Flow with Different Boundary Conditions

The numerical results of air movement in rooms are compared using the four different boundary conditions as described above:

1. simplified slit and k, ε calculated from equation (10)
2. velocities, k and ε from measurements (ε calculated from integral length scale)
3. velocities, k and ε from measurements (ε calculated from turbulence spectrum)
4. velocities from measurements and k, ε calculated from equation (10).

Profiles of velocity, turbulent kinetic energy and dissipation rate near the center plane of the room are shown in figure 5 for the y-direction.
The simplified slit boundary condition yields smaller velocities in the jet area and higher velocities in the occupied zone. Velocity profiles for the other three boundary conditions look similar. The simple turbulence boundary condition (Tu = 10%) gives the highest maximum velocity because the initial turbulence intensity is much smaller than the measured one. The maximum velocity calculated with the integral length scale boundary condition is higher than that with the turbulence spectrum. This is caused by the higher initial dissipation rate (see figure 4), which results in a lower level of turbulence in the center of the room as shown in the turbulence profile. The turbulent kinetic energy and rate of dissipation again show great differences between the simplified slit and the other three boundary conditions.
The profiles in a y-plane as shown in figure 6 indicate the same tendency. It is remarkable, that the results based on measured turbulence data are very similar to the results using the simple turbulence boundary condition. Only the simplified slit results in different velocity and turbulent kinetic energy profiles. The dissipation rate at the side wall is also greater because of the larger turbulent kinetic energy gradients.

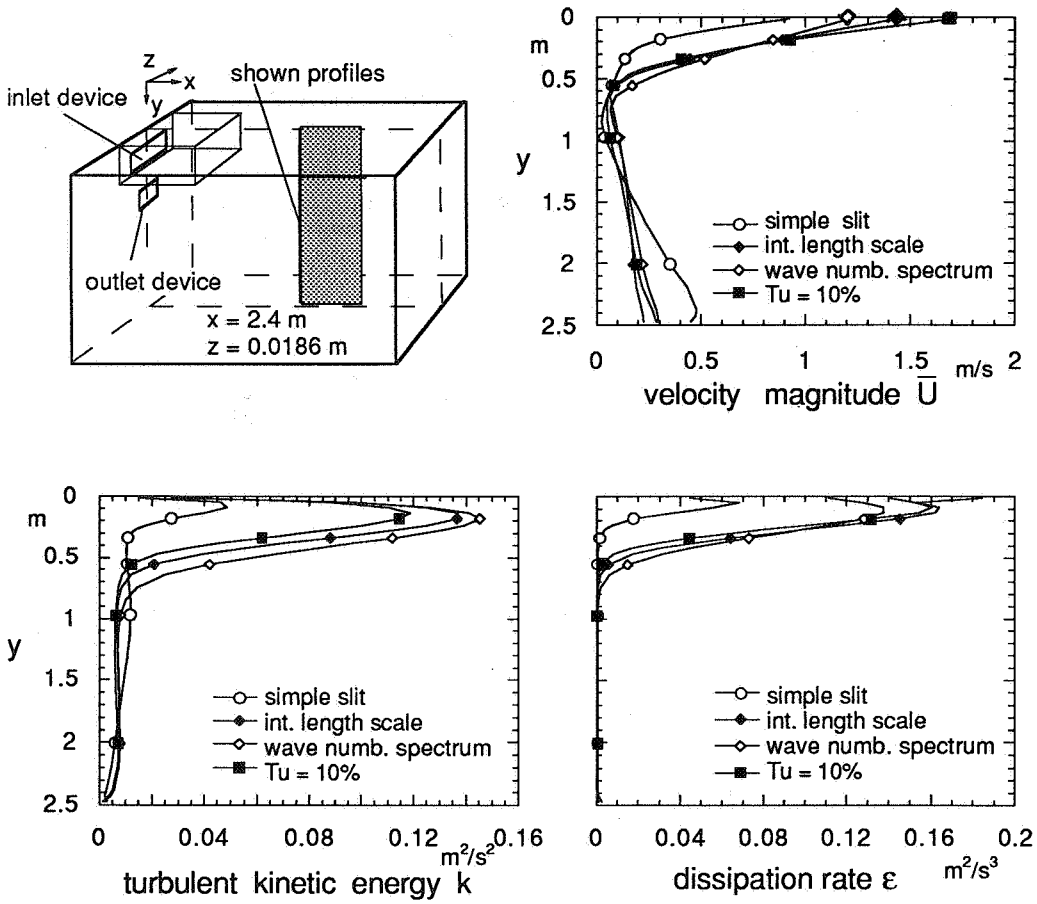

Figure 5: Profiles of velocity, k and ε from numerical simulations with different boundary conditions in a vertical plane of the room

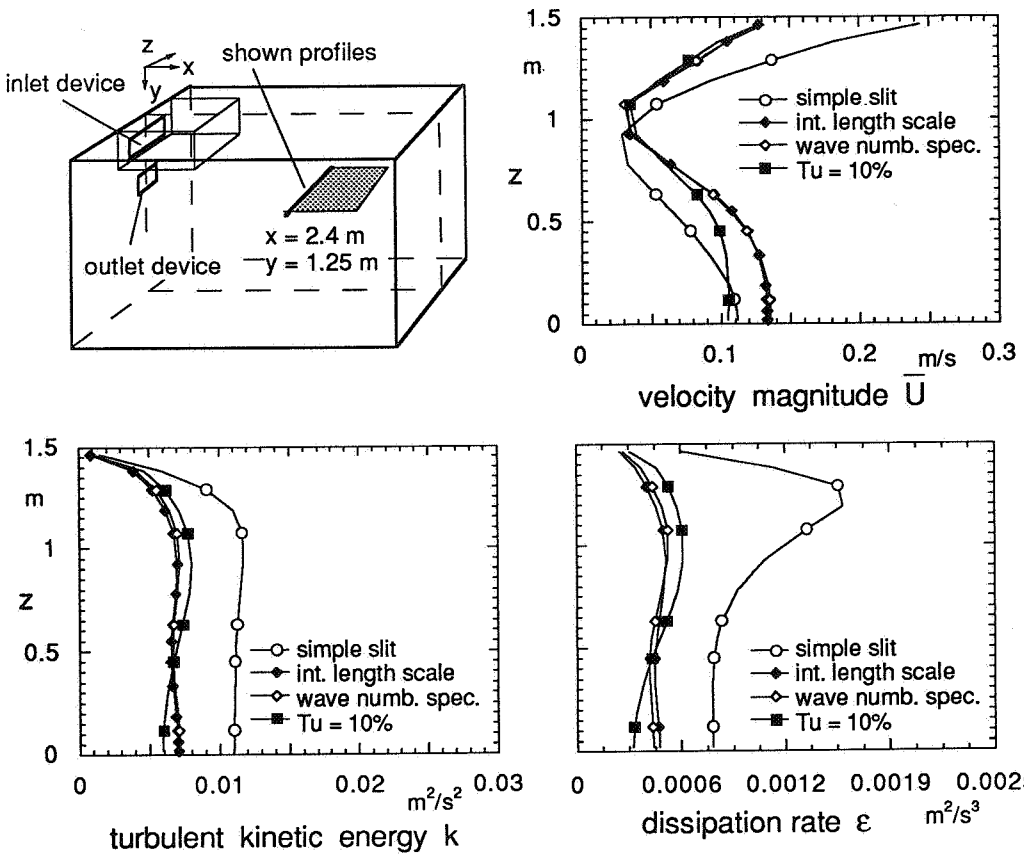

Figure 6: Profiles of velocity, k and ε from numerical simulations with different boundary conditions in a horizontal plane of the room

4. Conclusions

The evaluation of the dissipation rate of turbulent kinetic energy from measured velocities using two different models yields large quantitative differences, but the shape of the profiles is nearly the same. A general problem using the box method for the definition of boundary conditions is to determine the dimensions of the box. The box should be large enough so as to exclude the small flow structure of the real inlet from the calculation domain, but not too large, so as to avoid repercussion of the room air flow.

The comparison of numerical calculations using different boundary conditions has shown that the influence of the turbulence boundary condition is small compared with the influence of the inlet model, i.e. box method or simplified slit. The simplified slit model yields turbulent kinetic energies in the occupied zone two times larger than those resulting from the box method. The difference in these results significantly effects the PD value (percentage of dissatisfied) introduced by Fanger.

5. References

/1/ Ewert, M.; Zeller, M.; Turbulence Parameters at Supply Opening; Research Item 1.43, 1991, Annex 20 Report

/2/ Lemaire, A.D.; Testrooms, Identical Testrooms; Research Item 1.03, 1988, Annex 20 Report

/3/ Nielsen, P.; Selection of Air Terminal Device; Research Item 1.2, 1988, Annex 20 Report

/4/ Rotta, J.C.; Vollmers, H.; Ähnliche Lösungen der Differentialgleichungen für gemittelte Geschwindigkeiten, Turbulenzenergie und Turbulenzlänge; Forschungsbericht DLR (1976) 24

/5/ Rotta, J.O.; Turbulente Strömungen; B.G. Teubner Stutgart (1972)

/6/ Hinze, J.C.; Turbulence; McGraw Hill Inc.; New York and London (1975)

/7/ FLUENT. Creare Inc., PO Box 71, Hannover NH 03755 USA